

# Simultaneous Multi-Wavelength Observations of the TeV Blazar Mrk 421 during February – March, 2003: X-Ray and NIR Correlated Variability \*

Alok C. Gupta<sup>1,3</sup>, B. S. Acharya<sup>2</sup>, Debanjan Bose<sup>2</sup>, Varsha R. Chitnis<sup>2</sup> and Jun-Hui Fan<sup>1</sup>

<sup>1</sup> Center for Astrophysics, Guangzhou University, Guangzhou 510006, China; [acgupta30@gmail.com](mailto:acgupta30@gmail.com)

<sup>2</sup> Tata Institute of Fundamental Research, Homi Bhabha Road, Colaba, Mumbai - 400 005, India

<sup>3</sup> Aryabhata Research Institute of Observational Sciences (ARIES), Manora Peak, Nainital - 263129, India

Received 2007 October 24; accepted 2007 December 27

**Abstract** We report the result of simultaneous multi-wavelength observations of the TeV blazar Mrk 421 during February – March 2003. We observed Mrk 421 using the Pachmarhi Array of Čerenkov Telescopes (PACT) of Tata Institute of Fundamental Research at Pachmarhi, India. Other simultaneous data were taken from the literature and public data archives. We have analyzed the high quality X-ray (2–20 keV) observations from the NASA Rossi X-Ray Timing Explorer (RXTE). We obtained a possible correlated variability between X-ray and J band ( $1.25\ \mu$ ) near infrared (NIR) wavelength. This is the first case of X-ray and NIR correlated variability in Mrk 421 or any high energy peaked (HBL) blazar. The correlated variability reported here indicates a similar origin for the NIR and X-ray emissions. The emission is not affected much by the environment of the surrounding medium of the central engine of Mrk 421. The observations are consistent with the shock-in-jet model for the emissions.

**Key words:** galaxies: active — galaxies: blazars: general — galaxies: blazars: individual: Mrk 421

## 1 INTRODUCTION

A small subgroup of radio-loud active galactic nuclei (AGNs) shows significant flux variability in their overall electromagnetic (EM) spectrum and a variable polarization, and their radiation at all wavelengths is predominantly non-thermal. They are known as blazars, which is a collective name for the subclasses BL Lac objects, optically violent variables (OVVs), high polarization quasars (HPQs) and flat spectrum radio quasars (FSRQs) of radio-loud AGNs. On the unified model of radio-loud AGNs based on the angle between the line of sight and the emitted jet from the source, the blazars jets make angle  $< 10^\circ$  from the line of sight (Urry & Padovani 1995). The blazars emit radiation in the whole EM spectrum and this gives an excellent opportunity to study their spectral energy distribution (SED). It has been found from observations that the blazar SED shows two peaks, a first component peaking anywhere from IR to optical in the so called red blazars or low energy blazars (LBLs) or radio selected blazars (RBLs), and at UV/X-ray in so called blue blazars or high energy blazars (HBLs) or X-ray selected blazars (XBLs), its origin is synchrotron emission from high energy electrons in the jet. On the other hand, a second component extends up to  $\gamma$ -rays, and peaks at GeV energies in RBLs and at TeV in XBLs. The EM emission is dominated by

---

\* Supported by the National Natural Science Foundation of China.

synchrotron radiation at low-energies and by inverse Compton at high-energies (Coppi 1999; Sikora et al. 2001; Krawczynski 2004).

Mrk 421 is the nearest detected TeV BL Lac object (redshift  $z = 0.031$ ). It was first noted to be an object with blue excess which later turned out to be an elliptical galaxy with a bright point-like nucleus (Ulrich et al. 1975). Since the energy of its synchrotron peak is higher than 0.1 keV, it is classified as an HBL. Mrk 421 was the first extragalactic object discovered at TeV energies (Punch et al. 1992). It was later confirmed by the *high energy gamma-ray astronomy* (HEGRA) group (Petry et al. 1996). It is also one of the TeV blazars detected by the *energetic gamma-ray experiment telescope* (EGRET) instrument in the 30 MeV – 30 GeV energy range by the *Compton gamma-ray observatory* (CGRO) (Thompson et al. 1995). Mrk 421 has been detected by other detectors including the *imaging Compton telescope* (COMPTEL) on board CGRO at the  $3.2\sigma$  level in the 10–30 MeV energy range (Collmar et al. 1999), and the *solar tower atmosphere Čerenkov effect experiment* (STACEE) in the 140 GeV energy band (Boone et al. 2002).

Variability in Mrk 421 has been studied in all EM regions in isolation. An exhaustive compilation of radio data at 22 and 37 GHz, spanning for about 25 years, for several extragalactic sources including Mrk 421 was reported by Taräsranta et al. (2004, 2005). NIR data of several blazars including Mrk 421 extending about three decades were given by Fan & Lin (1999). A systematic and comprehensive study of this source was done by Gupta et al. (2004) in the same period of the campaign for which the present paper is written. In the compiled long-term optical data, variation of 4.6 mag was reported by Stein et al. (1976) and rapid variability of 1.4 mag in 2.5 hours was reported by Xie et al. (1988). There are several simultaneous X-ray and gamma-ray as well as multi-wavelength campaigns for the source (Makino et al. 1987; Macomb et al. 1995; Takahashi et al. 2000; Katarzynski et al. 2003; Blazejowski et al. 2005).

In the present paper, we aim to search for correlated multi-wavelength variability in Mrk 421. This kind of study will hopefully be an important tool for understanding the emission mechanism of blazars. This paper is structured as follows. In Section 2 we present the multi-wavelength observations and data reduction. Sections 3 and 4 give the results and discussion, respectively.

## 2 OBSERVATIONS, DATA AND THE DATA REDUCTION

### 2.1 TeV Observations with PACT

We have used Pachmarhi Array of Čerenkov Telescopes (PACT), for observation of Mrk 421 in TeV gamma-rays. PACT is located in Central India (latitude  $22^{\circ} 28' N$ , longitude  $78^{\circ} 25' E$ , altitude 1075 m). We use wavefront sampling technique to detect TeV  $\gamma$ -rays from astronomical sources. There are 24 telescopes spread over an area of  $80\text{ m} \times 100\text{ m}$ . Each telescope has seven para-axially mounted parabolic mirrors ( $f/d \sim 1$ ) of diameter 0.9 m with a PMT (EMI 9807B) mounted at the focus of each mirror. Each telescope is independently steerable, and is controlled remotely and monitored throughout the observation (Gothe et al. 2000). The entire array is sub-divided into four sectors with six telescopes in each. Each sector has its own data acquisition system (DAQ) where data on real time, relative arrival time of PMT pulses (using TDCs), and photon density (using ADCs) are recorded. A Master DAQ at the center of the array is also used for recording information of an event relevant to the entire array. Seven PMT pulses of a telescope are linearly added to form one telescope pulse for trigger generation. Data recording is initiated when a coincidence of four out of any six telescope pulses generates an event trigger for a sector. Typical trigger rate was about 1–3 Hz per sector. The details of this array can be found in Bhat et al. (2000) and Majumdar et al. (2003).

Observations are carried out in ON-OFF mode on clear moonless nights. In 2003, from February 26 to March 5, there was a world-wide multi-wavelength campaign of this source including PACT. During these nights two of the four sectors were aligned along the source direction and the remaining two were looking at a background region simultaneously. The background region is chosen to be a dark region with the same declination as the source but with a different RA, and is chosen in such a way that there is substantial overlap of zenith angle range between the source and background runs. A typical run lasts about 1–3 hours. The sectors that look at source and background were interchanged on a daily basis.

A number of preliminary checks were carried out on the data before doing the actual analysis. It was found that data taken on February 26 and 27 and on March 3 and 5 were bad and therefore were rejected. Observations taken on February 28, and March 1, 2 and 4 are analyzed. The arrival direction of each shower is determined by reconstructing the shower front using the relative arrival times of Čerenkov photons at various telescopes (or PMTs). The Čerenkov photon front is then fitted with a plane, whose normal defines

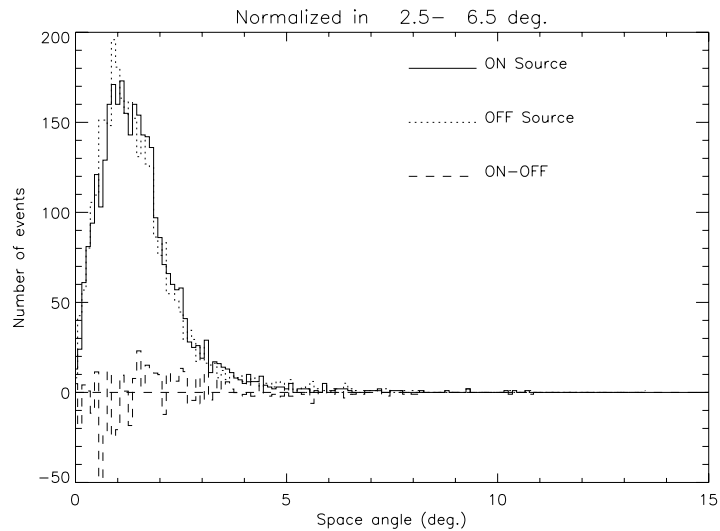


**Fig. 1** Space-angle distribution of source and background events for a typical run.

the direction of the shower axis. Then, for each shower or event, this angle is used to estimate the angle between the directions of the shower axis and the source. Thus the space angles are obtained for all the events for the source as well as the background runs. The space angle distributions of the source runs are compared with the respective background runs over the same zenith angle region. Due to some technical problem the source and background runs of same night could not be compared and each source run is compared with the background run of the previous or following night when the geometry of the telescope setup is also same for the source and background runs. For this comparison, the shapes of space angle distributions in  $2.5^\circ$  to  $6.5^\circ$  region of source and background were normalized, as we do not expect any signal beyond  $2.5^\circ$  (Majumdar et al. 2003). Normalization of distributions corresponding to the background with that of the source is necessary as these two data sets were taken at different times. Differences between the number of source and normalized background events within  $2.5^\circ$  give the estimate of  $\gamma$ -ray events.

Figure 1 shows the space angle distributions for a typical pair of source and background runs. Details of the analysis procedure are given in Bose et al. (2005). During the campaign nights no excess of events over the background is detected in any of those four nights, implying that the  $\gamma$ -ray flux is close to or below the sensitivity limit of PACT.

Čerenkov photon showers initiated by  $\gamma$ -rays and protons were simulated using CORSIKA air shower simulation code (Heck et al. 1998) to estimate the trigger rate, energy threshold, collection area, etc., for the PACT setup. For  $\gamma$ -rays incident vertically the energy threshold, defined as the peak of the differential rate curve, is estimated to be 750 GeV and the corresponding collection area is  $1.58 \times 10^5 \text{ m}^2$ . For Mrk421, which is at an angle of  $20^\circ$  w.r.t. the zenith the energy threshold is estimated to be 1.2 TeV and the collection area,  $1.8 \times 10^5 \text{ m}^2$ .

## 2.2 X-Ray Observations with RXTE

We have extracted archival data sets corresponding to this multi-wavelength campaign under the guest observing program 80172. RXTE has two types of detectors viz, Proportional Counter Array (PCA) and High-Energy X-ray Timing Explorer (HEXTE) on-board along with the All Sky Monitor (ASM). The PCA consists of five identical xenon filled proportional counter units (PCUs) covering the energy range 2–60 keV. During these observations only PCU 0 and PCU 2 were used. Since PCU 0 lost pressure in the top veto at the beginning of Epoch 5, we have used only data from PCU 2. The HEXTE consists of two clusters of phoswich scintillation detectors covering the energy range 15–250 keV, but is less sensitive. We will not discuss the HEXTE data here. The ASM consists of three xenon filled position sensitive proportional counters with a field of view of  $6 \times 90$  degrees. It covers 80% of the sky every 90 minutes and spans the energy range 2–10 keV.

We analyzed Standard 2 PCA data which have a time resolution of 16 s with energy information in 128 channels. The data reduction is done with FTOOLS (version 5.3.1) distributed as part of HEASOFT (version 5.3). For each of the observations, the data were filtered using standard procedure for faint sources given in the RXTE Cook Book. For extraction of background, the model appropriate for faint sources (*pca\_bkgd\_cmfaint17\_eMv20031123.mdl*) was used. Light curves were extracted from data in three energy bands: 2–9, 9–20 and 20–40 keV. Background light curves were also extracted and subtracted from the source light curves. We obtained the ASM data from the MIT archive. The light curves were generated using the one-day averages.

### 2.3 Data from Literature: Multi-Wavelength Data

The near-infrared data in the J band used in the present paper are taken from Gupta et al. (2004). The observations were done using the 1.2 meter optical/NIR telescope at Gurushikhar observatory, Mount Abu, India with NICMOS-3 detector and a J band filter. The details about the NIR observations and data reduction are given in Gupta et al. (2004).

The radio data are taken from the recent paper by Taräsranta et al. (2005). They observed the source at 22 and 37 GHz during the campaign using their 17.7 meter Metsähovi radio telescope. Details about radio data are given in Taräsranta et al. (1998).

## 3 RESULTS

### 3.1 Multi-Wavelength Light Curves

Figure 2 gives the radio to gamma-ray light curves during the multi-wavelength campaign 2003 February 25 – March 05. The data plotted here for the different EM bands are daily averages. The daily average of a given date is reported at 00<sup>h</sup>00<sup>m</sup>00<sup>s</sup> UT. The radio flux seems to be in a stable state, implying that the variability timescale may be longer than the duration of the campaign. On the other hand gamma-ray data are noisy. The figure shows highly correlated variability among the different energy bands of the PCA data.

Figure 3 gives the NIR and X-ray light curves (with 5 minutes binning) for the observations during 2003 February 26 – March 05. The X-ray coverage was much longer than the NIR coverage, so we have selected that portion of the X-ray data which was approximately simultaneous with the NIR data. For this plot the PCA data of two energy bands, 2–4 keV and 4–9 keV, are combined.

### 3.2 Cross Correlation Function (ZDCF)

We computed the ZDCF (Z-transformed discrete correlation function) (Alexander 1997) for the light curves in X-ray and NIR bands. ZDCF is a method for determining the cross-correlation function (CCF) of light curves in different energy bands with unevenly sampled data, which makes use of the Fisher's z-transform of the correlation coefficient. Fisher's z-transform of the linear correlation coefficient,  $r$ , is used to estimate the confidence level of the measured correlation. This method attempts to correct the biases that affect the original DCF (discrete correlation function) by using equal population binning. The ZDCF involves the following three steps:

- (i) All possible pairs of observations,  $(a_i, b_j)$ , are sorted according to their time-lag  $t_i - t_j$ , and binned into equal population bins.
- (ii) Each bin is assigned its mean time-lag and the intervals above and below the mean that contains  $1\sigma$  of the each point.
- (iii) The correlation coefficients of the bins are calculated and z-transformed. The error is calculated in  $z$ -space and transformed back to  $r$ -space.

The time-lag corresponding to the ZDCF is assumed as the time delay between the two components. This function is much more efficient in detecting any correlation present, also it takes care of the data gaps. The ZDCF seems to peak at a negative lag  $-3$  days, which means that the X-ray variability lags behind the NIR variability. Since the dataset is sparse and the value of ZDCF (max) is  $\sim 0.5$ , so, we claim it as a weak correlated variability. It will be interesting to see with more such observations obtained in future.

The ZDCFs are plotted in Figure 4 for the three combination of light curves plotted in Figure 3. The cross-correlation coefficient max (ZDCF) and time lag  $\tau$  for each combination of light curves are as follows:

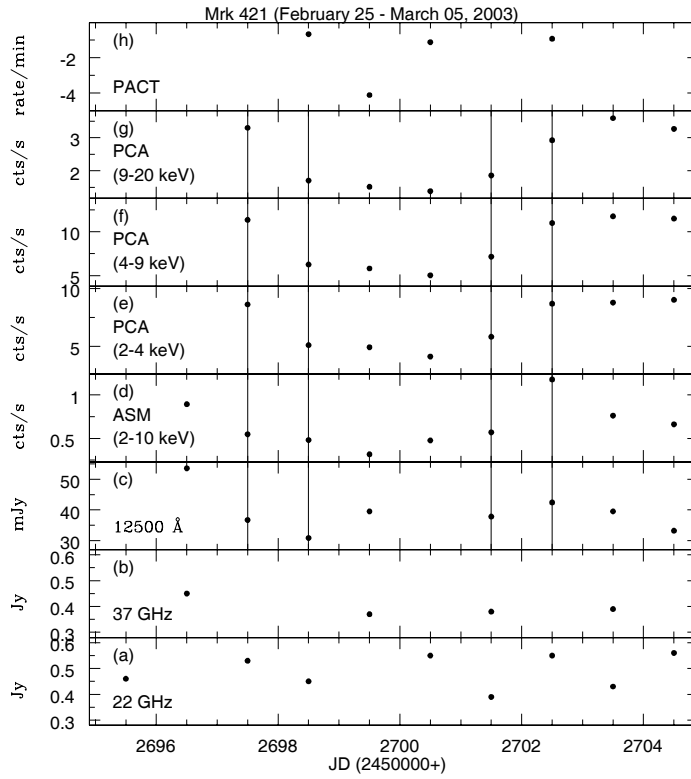


**Fig. 2** Multi-wavelength data of Mrk 421 as a function of time for all bands from radio to gamma-rays observed during the period 2003 February 25–March 05. Vertical lines in panels c-g show simultaneous variations in the NIR and X-ray bands. In general, the uncertainties are smaller than the size of the symbols, so the error bars have been omitted.

- (i) For PCA (2–9 keV) vs 12500 Å  $\max(\text{ZDCF}) = 0.530^{+0.1715}_{-0.1515}$ ,  $\tau = -3.02$  days
- (ii) For PCA (9–20 keV) vs 12500 Å  $\max(\text{ZDCF}) = 0.460^{+0.1915}_{-0.1728}$ ,  $\tau = -3.02$  days
- (iii) For PCA (2–9 keV) vs PCA (9–20 keV)  $\max(\text{ZDCF}) = 0.747^{+0.0173}_{-0.0168}$ ,  $\tau = -0.11$  days

A visual inspection of the data in Figure 2 shows a strong correlation between the NIR and X-ray bands on JD 2452697.5, 2452698.5, 2452701.5 and 2452702.5. In particular, the source tended to reach a faint stage at JD 2452697.5 and to show some flaring activity at JD 2452701.5, and the positive correlation is seen in both the flaring and quiescent states. At JD 2452699.5, the NIR data showed an anti-correlation with the PCA data (this anti-correlation is responsible for lowering the correlation coefficients stated above). On March 01, observations could not be taken in the NIR J band due to bad weather condition. So, there is no NIR data for JD 2452700.5 in panel c of Figure 2.

### 3.3 Spectral Energy Distribution (SED)

The SED of Mrk 421 is plotted in Figure 5 in the form  $\log \nu F_\nu$  vs.  $\log \nu$ . All the frequencies shown here are observed frequencies. The synchrotron component of the SED was fitted using the NIR and X-ray data with a parabolic function,

$$y = Ax^2 + Bx + C. \quad (1)$$

The synchrotron peak frequency is determined by  $\nu_{\text{peak}} = -B/2A$ . Accordingly we have  $\nu_{\text{peak}} = 16.30$ . It was noticed by Nieppola et al. (2006) that using the simple parabolic fit for HBLs produces some error. For HBLs, the synchrotron peak is expected close to soft X-ray band which declines very rapidly. Thus, the true peak frequency will be slightly higher than the reported value.

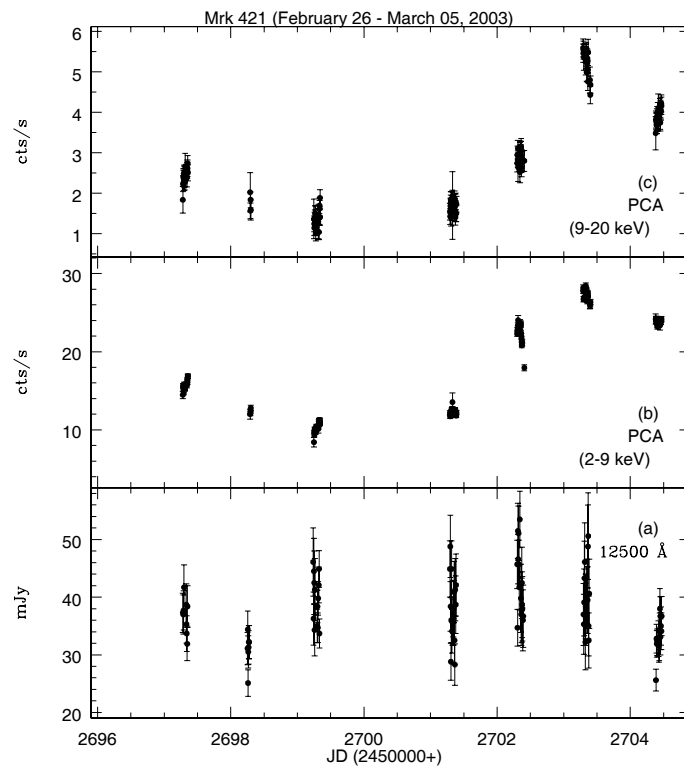


**Fig. 3** NIR and X-ray bands data of Mrk 421 as a function of time observed during the period 2003 February 26 – March 05.

#### 4 DISCUSSION

We have found here evidence for a possible correlation between X-ray and NIR wavelengths in the HBL blazar, Mrk 421.

So far, correlated X-ray and NIR variation was observed in a LBL blazar, 3C 273, a flat spectrum radio quasar (FSRQ) (McHardy et al. 1999). For another LBL blazar, AO 0235+164, simultaneous radio and optical variability was reported during the optical outbursts that occurred in 1975, 1979 and 1997 (MacLeod et al. 1976; Ledden et al. 1976; Rieke et al. 1976; Balonek & Dent 1980; Webb et al. 2000). On the other hand, no correlation was found in the radio and optical emissions of another LBL blazar, S5 0716+714 (Ostorero et al. 2006). In a multi-wavelength campaign of the LBL blazar 3C 279 reported by (Wehrle et al. 1998), correlated variability in X-ray (PCA) and EGRET CGRO is seen without any time lag; while the UV leading the gamma-ray by  $\sim 2.5$  days. Since the UV and gamma-ray data were small in size, this observation may not be so reliable.

Edelson et al. (1995) have reported correlated emission between X-ray, UV and optical emissions from PKS 2155–304 (an HBL BL Lac object). In another multi-wavelength campaign of PKS 2155–304 covering 10 days, Urry et al. (1997) reported the X-ray flare leading the EUV flare by one day and the UV flare by two days. McComb et al. (1995) and Maraschi et al. (1999) presented simultaneous X-ray and  $\gamma$ -ray flares in Mrk 421 in two different campaigns. In another campaign of Mrk 421 in 1998 (Takahashi et al. 2000), a complex variability and with positive and negative lags were found which authors stated may not be real. If the lags of both signs are real, then it would imply that the timescales of particle acceleration and X-ray cooling are similar. Katarzynski et al. (2003) showed a well defined correlation between observed radio outburst in Mrk 421 with a corresponding X-ray outburst and a  $\gamma$ -ray flare in TeV range. In simultaneous TeV and optical observations of the blazar 1406–076, the optical flare leading the gamma-ray flare by  $\sim 1$  days (Wagner et al. 1995).

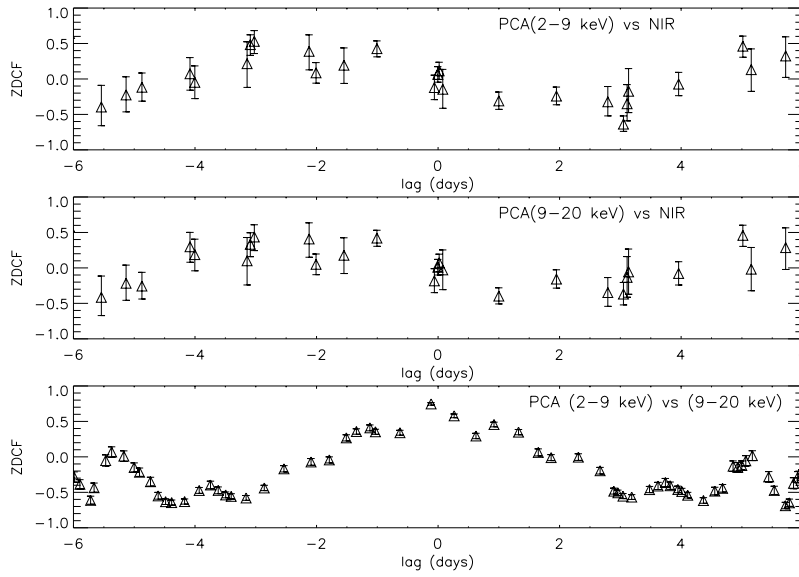


**Fig. 4** NIR and X-ray correlations. Positive lags imply that the second light curve lags the first.

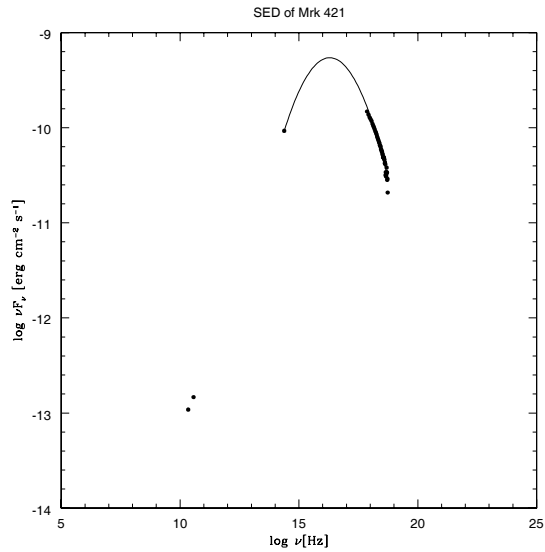


**Fig. 5** Spectral energy distribution (SED) of the Mrk 421.

In a recent paper, Villata et al. (2006) showed that the historical radio and optical light curves varied differently, and prominent and long-lasting outbursts were visible at various radio frequencies, the higher-frequency variations preceding the lower-frequency ones. After these, the optical flux became more variable, and the radio flux, less. The suggestion is that the optical and radio emissions come from two separate and un-aligned jet regions. The correlated emissions reported in several papers support models involving a single population of relativistic electrons responsible for the emissions.

One of the important question is “Where does the NIR radiation originate”? There are three possibilities: (i) emission from the circumstellar dust, (ii) emission from the accretion disk, (iii) synchrotron emission by relativistic electrons in the jet. The first two are external to the jet. The variability behavior

indicates a similar origin for the NIR and X-ray emission. The X-ray emission originates from synchrotron radiation by electrons in the AGN, as mentioned before.

From different multi-wavelength campaigns it has been noticed that variations at longer wavelengths are generally not seen during X-ray and  $\gamma$ -ray flaring events (Tosti et al. 1998 and references therein). Ghisellini & Maraschi (1996) showed that the overall emission of the BL Lac, Mrk 421 could be explained using a homogeneous SSC model, in which an equilibrium particle distribution results from balancing the continuum injection, cooling and particle escape. In this single population, the relativistic electrons emit synchrotron radiation up to the UV or X-ray band and soft photons up to the IR-optical bands undergo upscattering by the most energetic electrons to emit TeV  $\gamma$ -rays. However, Blazejowski et al. (2005) found TeV flares reached its peak days before the X-ray flare during a giant flare or outburst in 2004. The SED generated by Blazejowski et al. (2005) was not fitted with a one-zone synchrotron self-Compton (SSC) model but could be fitted well with multiple zones.

Following Ghisellini & Maraschi (1996), Marscher (1996) and other authors, we note that the lags in the multi-frequency light curves of Mrk 421 (of the order of hours between soft and medium X-ray photons, near simultaneous X-ray and  $\gamma$ -ray flares, IR leading X-rays by couple of days) require energy stratification in the source. Similar delays were noticed in 3C 279 (IR leads X-ray by  $0.75 \pm 0.25$  day) and in PKS 2155–304 (a day between EUV and X-rays, 2 days between UV and X-rays) and of the order of few hours between these (Edelson et al. 1995) as well. Frequency stratification and different time scales for the duration of these flares (shorter times for higher frequencies) are possible with the shock-in-jet model (Marscher 1996 and references therein).

Within the context of the shock-in-jet model of AGNs, we attribute the NIR emission component to the internal shock driven into the jet by the variation of the central engine. The correlated X-ray and NIR variability with time lag of few days is a strong probe of the jet emission not affected much by the environment of the surrounding medium. The anti-correlation seen in the NIR and soft X-ray light curve at JD 2452699.5 may be due to the reverse shock arising by the jet's collision with the surrounding medium.

**Acknowledgements** We thankfully acknowledge the referee for useful comments. The work of A. C. Gupta and J. H. Fan is supported by the National Natural Science Foundation of China (Grants 10573005 and 10125313). We gratefully acknowledge the use of RXTE data from the public archive of GSFC/NASA. Also, we are grateful to all the members of PACT collaboration for their respective contributions.

## References

- Alexander T., 1997, *Astronomical Time Series*, ed. D. Maoz, A. Sternberg, E. M. Leibowitz, Dordrecht: Kluwer, p.163
- Balonek T. J., Dent W. A., 1980, *ApJ*, 240, L3
- Bhat P. N. et al., 2000, *Bulletin of Astronomical Society of India*, 20, 455
- Blazejowski M., Blaylock G., Bond I. H. et al., 2005, *ApJ*, 630, 130
- Boone L. M., Hinton J. A., Bramel D. et al., 2002, *ApJ*, 579, L5
- Bose D. et al., 2005, 29th International Cosmic Ray Conference Proceedings, 4, eds. B. S. Acharya et al., p. 343
- Collmar W., Bennett K., Bloemen H. et al., 1999, *ApL&C*, 39, 57
- Coppi P. S. 1999, in workshop summary for the Cracow Workshop on Relativistic Jets in AGNs, ed. M. Ostrowski, M. Sikora, G. Madejski, M. Begelman, Jagellonian University Press, p. 333
- Edelson R., Krolik J., Madejski G. et al., 1995, *ApJ*, 438, 120
- Fan J. H., Lin R. G., 1999, *ApJS*, 121, 131
- Ghisellini G., Maraschi L., 1996, *ASP Conf. Series 110 on Blazar Continuum Variability*, eds. H. R. Miller, J. R. Webb, J. C. Noble, p. 436
- Gothe K. S. et al., 2000, *Indian Journal of Pure & Applied Physics*, 38, 269
- Gupta A. C., Banerjee D. P. K., Ashok N. M., Joshi U. C., 2004, *A&A*, 422, 505
- Heck D. et al., 1998, FZKA 6019 Forschungszentrum Karlsruhe (user manual of the computer code CORSIKA named "Extensive air shower simulation with the CORSIKA")
- Katarzynski K., Sol H., Kus A., 2003, *A&A*, 410, 101
- Krawczynski H., 2004, *New Astronomy Rev.*, 48, 376
- Ledden J. E., Aller H. D., Dent W. A., 1976, *Nature*, 260, 752
- Macomb D. J., Akerlof C. W., Aller H. D. et al., 1995, *ApJ*, 449, L99

- MacLeod J. M., Andrew B. H., Harvey G. A., 1976, *Nature*, 260, 751
- Makino F., Tanaka Y., Matsuoka M. et al., 1987, *ApJ*, 313, 662
- Majumdar P., Acharya B. S., Chitnis V. R. et al., 2003, *Astroparticle Physics*, 18, 339
- Maraschi L., Fossati G., Tavecchio F. et al., 1999, *ApJ*, 526, L81
- Marscher A. P., 1996, *ASP Conf. Series 110 on Blazar Continuum Variability*, eds. H. R. Miller, J. R. Webb, J. C. Noble, p. 248
- McHardy I., Lawson A., Newsam A. et al., 1999, *MNRAS*, 310, 571
- Nieppola E., Tornikoski M., Valtaoja E., 2006, *A&A*, 445, 441
- Ostorero L., Wagner S. J., Gracia J. et al., 2006, *A&A*, 451, 797
- Petry D., Bradbury S. M., Konopelko A. et al., 1996, *A&A*, 311, L13
- Punch M., Akerlof C. W., Cawley M. F. et al., 1992, *Nature*, 358, 477
- Rieke G. H., Grasdalen G. L., Kinman T. D. et al., 1976, *Nature*, 260, 754
- Sikora M., Madejski G., 2001, in *AIP Conf. Proc. 558, High Energy Gamma-Ray Astronomy*, ed. F. A. Aharonian, H. J. Völk (New York: AIP), p.463
- Stein W. A., O'Dell S. L., Strittmatter P. A., 1976, *ARA&A*, 14, 173
- Takahashi T., Kataoka J., Madejski G. et al., 2000, *ApJ*, 542, L105
- Taräsranta H., Achren J., Hanski M. et al., 2004, *A&A*, 427, 769
- Taräsranta H., Wiren S., Koivisto P. et al., 2005, *A&A*, 440, 409
- Thompson D. J., Bertsch D. L., Dingus B. L. et al., 1995, *ApJS*, 101, 259
- Tosti G., Fiorucci M., Luciani M. et al., 1998, *A&A*, 339, 41
- Ulrich M. H., Kinman T. D., Lynds C. R. et al., 1975, *ApJ*, 198, 261
- Urry C. M., Padovani P., 1995, *PASP*, 107, 803
- Urry C. M., Treves A., Maraschi L. et al., 1997, *ApJ*, 486, 799
- Villata M., Raiteri C. M., Balonek T. J. et al., 2006, *A&A*, 453, 817
- Wagner S. J., Mattox J. R., Hopp U. et al., 1995, *ApJ*, 454, L97
- Webb J. R., Howard E., Bentez E. et al., 2000, *AJ*, 120, 41
- Wehrle A. E., Pian E., Urry C. M. et al., 1998, *ApJ*, 497, 178
- Xie G.-Z., Lu R.-W., Zhou Y. et al., 1988, *A&AS*, 72, 163